Relativistic Fluid Modelling of the Gamma-Ray Binary LS 5039

D. Huber, R. Kissmann & O. Reimer

Institut für Astro- und Teilchenphysik, Leopold-Franzens-Universität Innsbruck, Austria

universität innsbruck

Abstract

LS 5039 is one of the best-observed gamma-ray binaries with non-thermal emission ranging from soft X-rays to VHE gamma-rays. Explaining the observed anti-correlation between the X-ray/VHE and the HE gamma-ray bands, while accounting for its complex spectral features, has become a challenge for current modelling efforts.
Here we present the application of a novel numerical model to LS 5039. We treat the particle acceleration and transport simultaneously to the pulsar- and wind interaction, which enables the consistent incorporation of a multitude of effects. With this, we were able to simulate LS 5039 with unprecedented complexity and provide first insights into turbulent phenomena in this source.

LS 5039

- Compact orbit: $3.9\,\mathrm{d}$, $e = 0.35$ | O-type star + Compact object [3]
- Anticorrelated emission bands: X-ray, LE, VHE vs. HE
- Multiple emission components: keV-MeV, GeV, TeV

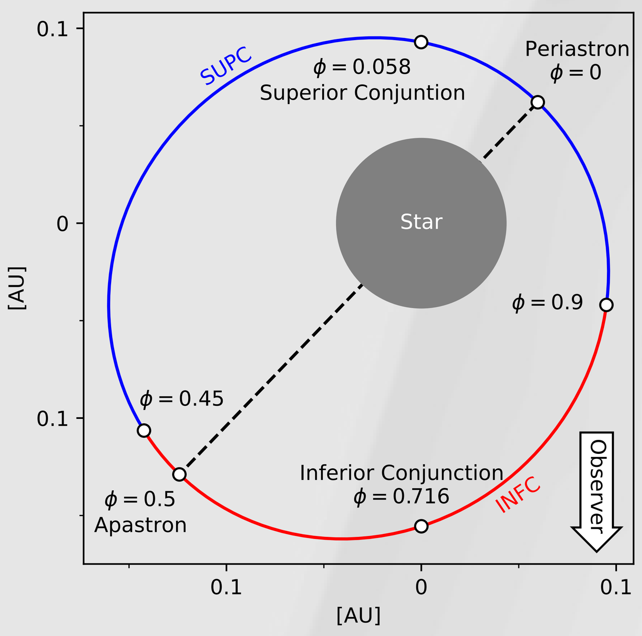

Fig 1: The LS 5039 orbit. [2]

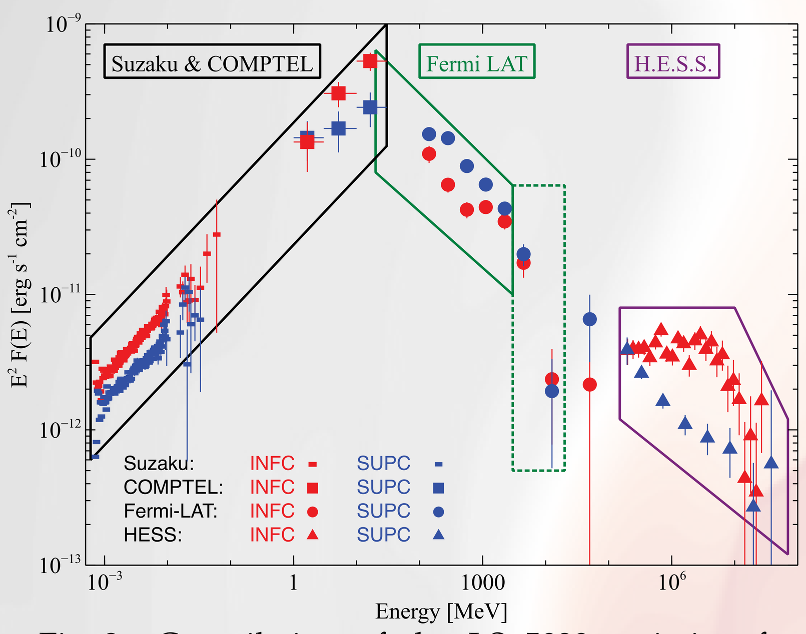

Fig 2: Compilation of the LS 5039 emission for different orbital-phase ranges. Credit: [4]

High-Mass Gamma-Ray Binary Models

Emission Scenarios

- Accretion driven microquasar [5]
- **Pulsar wind driven** [6] - favoured for most systems [7]
  - → Wind interaction → Shocks
  - → Acceleration of electrons from the pulsar wind
  - → Emission of gamma-rays

Radiative Processes

- Synchrotron emission
- Anisotropic inverse Compton scattering on stellar photons

Modulation

- Relativistic boosting
- Gamma-gamma absorption

Current models

- **Simplified wind interaction** and/or analytic estimations for accelerator locations
- Particle transport treated as post-processing, **neglecting dynamics** of the wind interaction

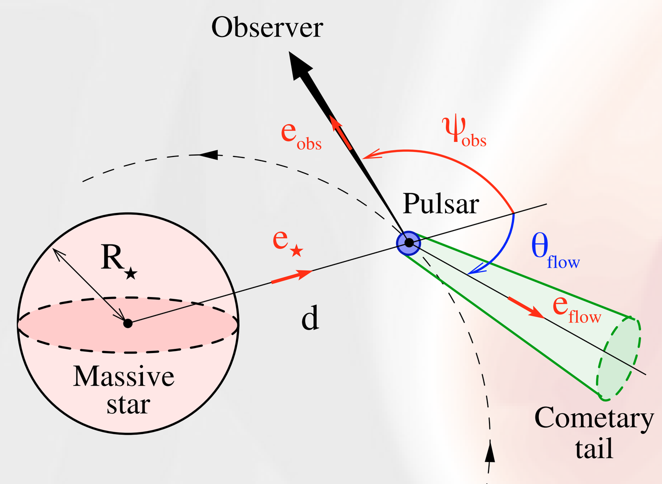

Fig 3: Geometry of the binary. Credit: [8]

Numerical Treatment

Space: Semi-discrete, finite-volume Godunov scheme using Cronos [9].

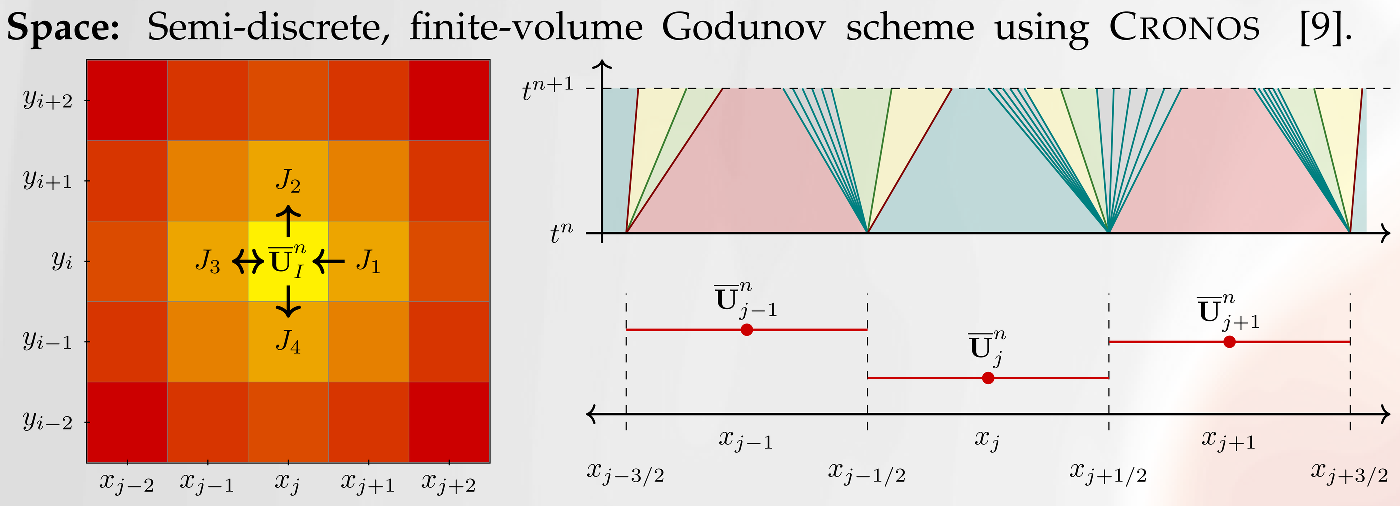

Fig 4: Left: Schematic representation of a finite volume scheme. Right: Godunov's idea - local Riemann problems at each cell-interface.

Energy: Semi-Lagrangian, conservative scheme [1]

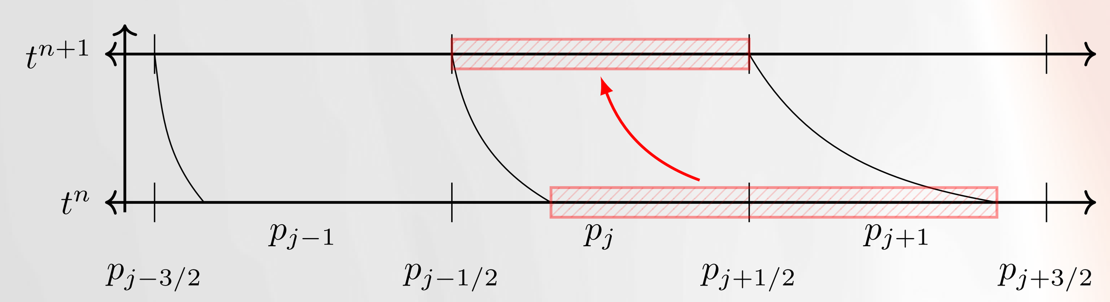

Fig 5: Schematic representation of a semi-Lagrangian solver; particles are transported along characteristic curves.

References

[1] D. Huber et al. A&A **646** (2021), A91. 2012.04975 [astro-ph.HE].
[2] D. Huber et al. arXiv e-prints (2021). 2103.00995 [astro-ph.HE].
[3] J. Casares et al. MNRAS **364**.3 (2005), 899. astro-ph/0507549 [astro-ph].
[4] Z. Chang et al. MNRAS **463**.1 (2016), 495. 1608.04589 [astro-ph.HE].
[5] V. Bosch-Ramon et al. IJMP D **18**.3 (2009), 347. 0805.4123 [astro-ph].
[6] L. Sironi et al. ApJ **741**.1 (2011), 39. 1107.0977 [astro-ph.HE].
[7] G. Dubus. A&A Rev. **21** (2013), 64. 1307.7083 [astro-ph.HE].
[8] G. Dubus et al. A&A **516** (2010), A18. 1004.0511 [astro-ph.HE].
[9] R. Kissmann et al. ApJS **236**.2 (2018), 53. 1806.09479 [astro-ph.IM].
[10] J. Takata et al. ApJ **790**.1 (2014), 18. 1406.6179 [astro-ph.HE].
[11] V. Bosch-Ramon. A&A **645** (2021), A86. 2012.11578 [astro-ph.HE].

Wind Interaction

Relativistic hydrodynamics

- Pulsar launches **relativistic wind** (here $v = 0.99\,c$)
- Fully 3D numerical simulation of the wind interaction in corotating, Cartesian coordinates [2]

$$\partial_t U + \nabla_j \mathbf{F}^j = S \qquad U = \begin{pmatrix} \rho W \\ \rho W h u^i \\ \rho h W^2 - p \end{pmatrix} \; \mathbf{F}^j = \begin{pmatrix} \rho u^j \\ \rho h u^i u^j + p\delta^{ij} \\ m^j \end{pmatrix}$$

Extended wind-collision region

- Formation of **shocks**: bow, Coriolis, and secondary shocks
- **Instabilities** strongly affect the shock structure and trigger turbulent mixing

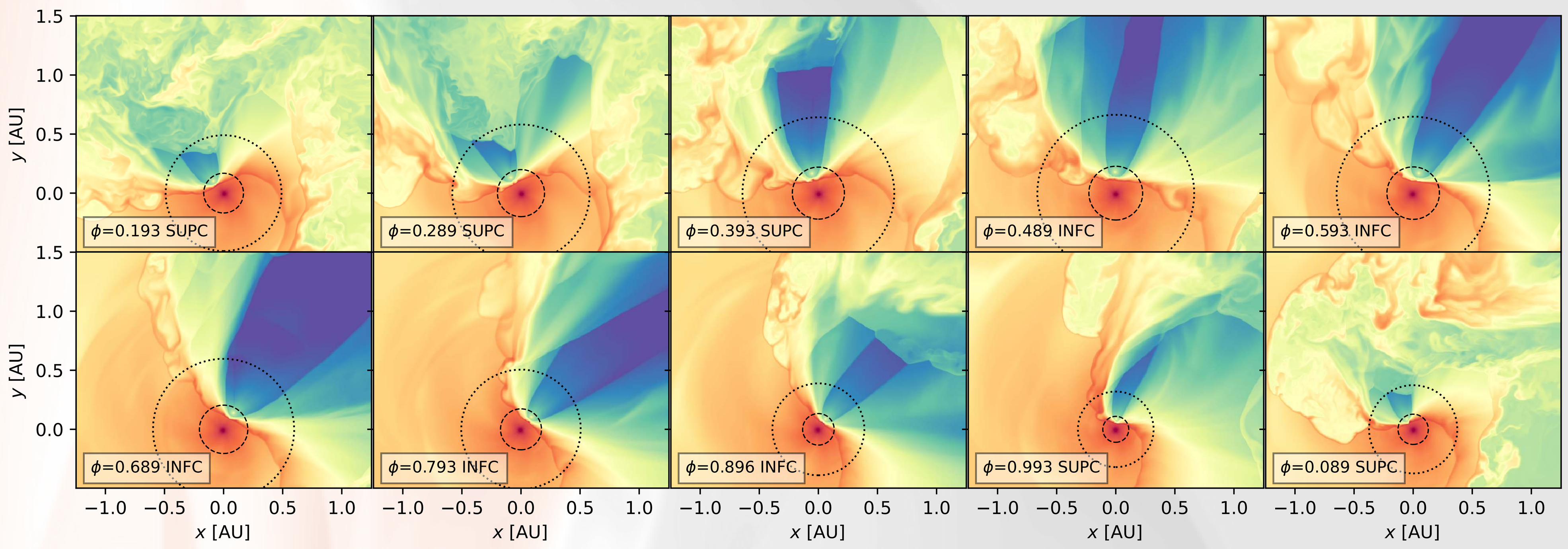

Fig 6: Fluid density of the wind collision region for different orbital phases. [2]

Particle Transport

Particle Injection

- Electron **acceleration** at shocks $\nabla_\mu u^\mu < \delta_{\mathrm{sh}}$
- Depending on local fluid conditions [1]
- Maxwellian (MW) $\propto \gamma^2 \exp\left(-\gamma/\gamma_t\right)$
- Powerlaw (PL) $\propto \gamma^{-s}$ for $\gamma_{\min} < \gamma < \gamma_{\max}$

Transport

- **Simulateneous** treatment with the hydrodynamics
- Synchrotron losses → assumption: $w_{\mathrm{mag}} \propto e_{\mathrm{internal}}$
- Inverse Compton losses $w_{\mathrm{rad}} \propto d_\star^{-2}$

$$\underbrace{\nabla_\mu \left(u^\mu \mathcal{N}\right)}_{\text{Spatial advection}} + \partial_\gamma \left(\underbrace{-\frac{\nabla_\mu u^\mu}{3}\gamma \mathcal{N}}_{\text{Adiabatic losses}} + \underbrace{\dot{\gamma}_{\mathrm{rad}} \mathcal{N}}_{\text{Radiative losses}} \right) = 0$$

Fig 7: Electron density for different orbital phases at $\gamma = 3 \times 10^3$ (top) and $\gamma = 10^7$ (bottom). [2]

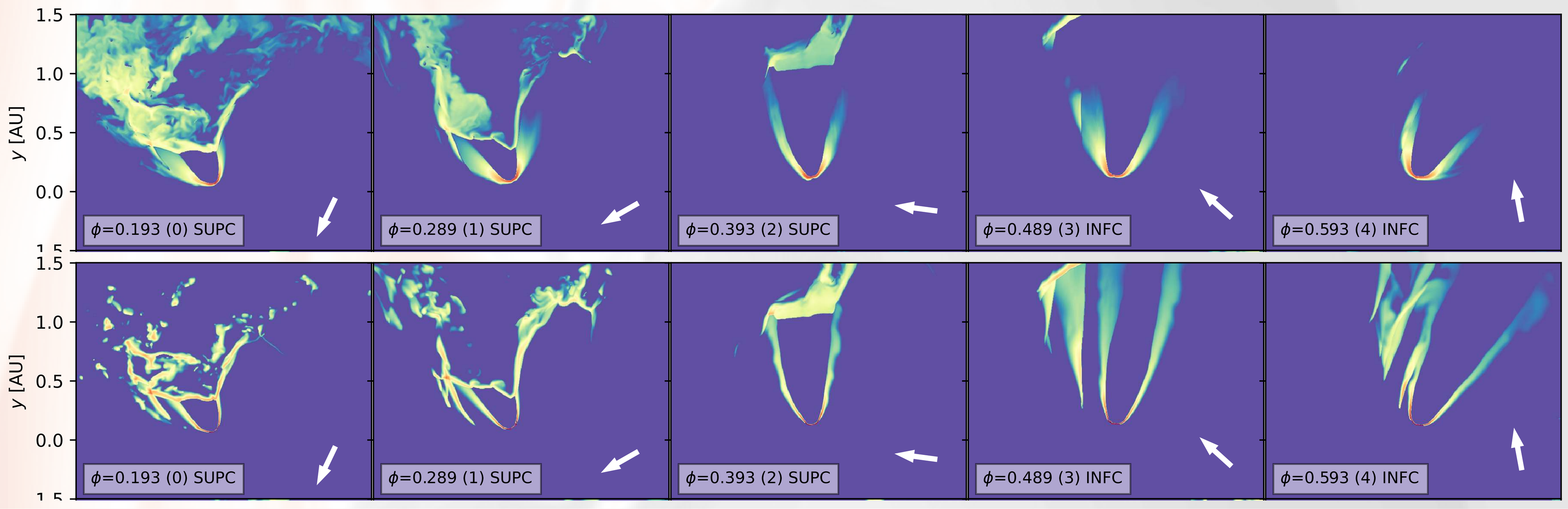

Emission Predictions

Spectrum

Main spectral features reproduced:

- PL + Synchrotron → keV-MeV
- MW + IC → GeV
- PL + IC + $\gamma\gamma$ absorption → TeV
- Missing GeV contribution
  - → Pulsar magnetosphere [10]
  - → Cold pulsar wind [11]

Lightcurves

- Reproducing HE/VHE anticorrelation
- Wrong behaviour for keV-MeV
  - → Assumptions on magnetic field too simple
  - → **RMHD** needed
- Turbulence induced variability up to $\sim 20\%$

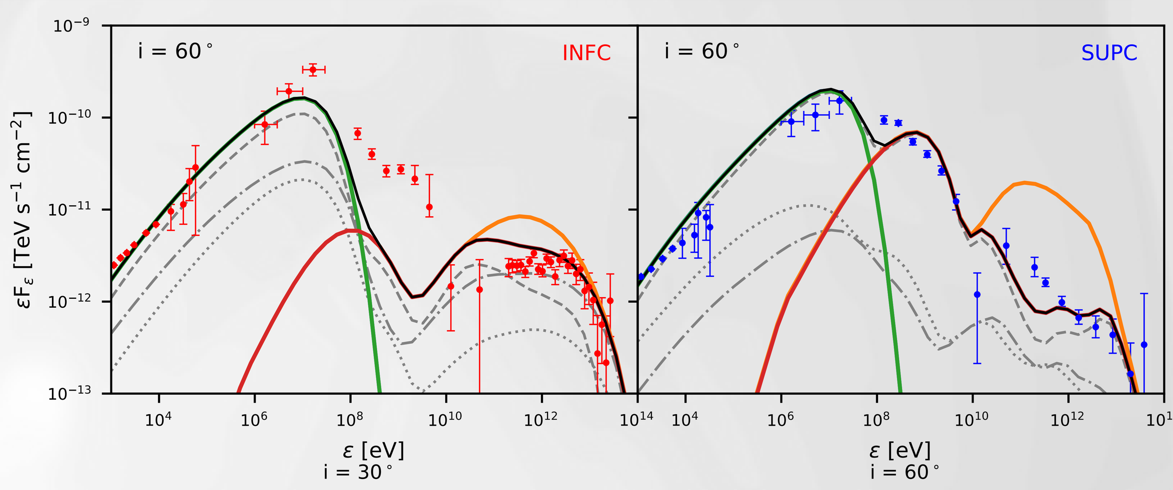

Fig 8: Simulated LS 5039 spectrum for a system inclination of $i = 60°$. [2]

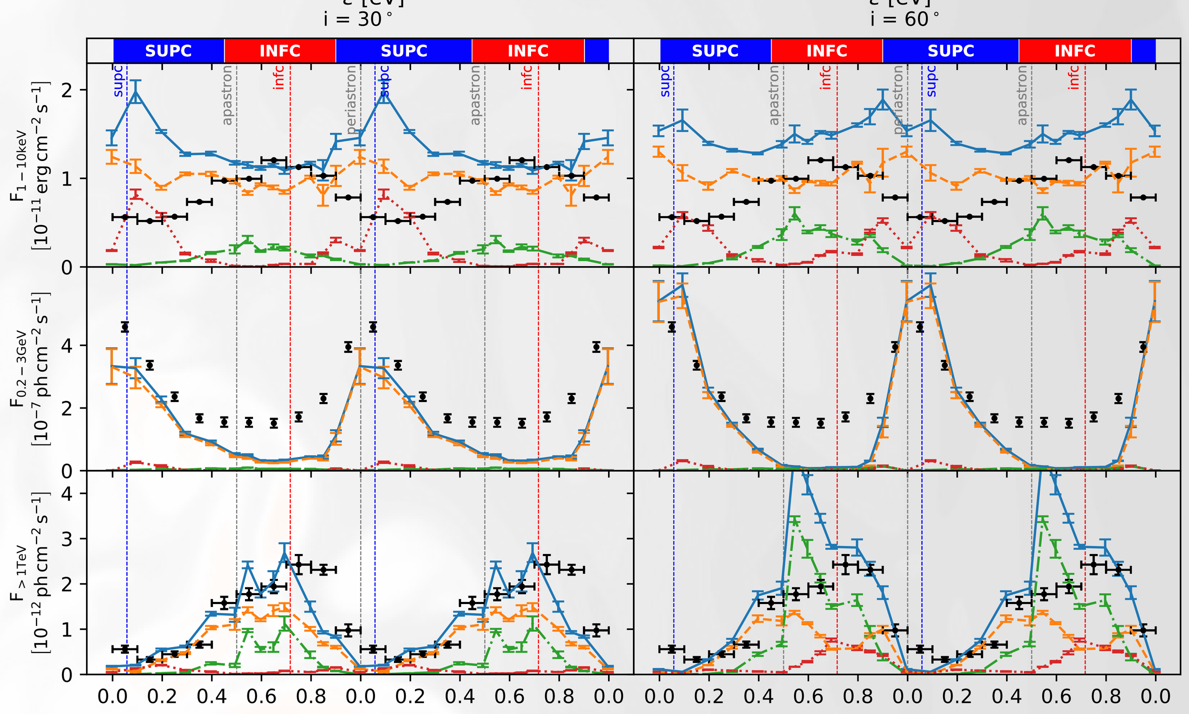

Fig 9: Simulated LS 5039 lightcurves for different bands and inclinations. [2]

Emission Projections

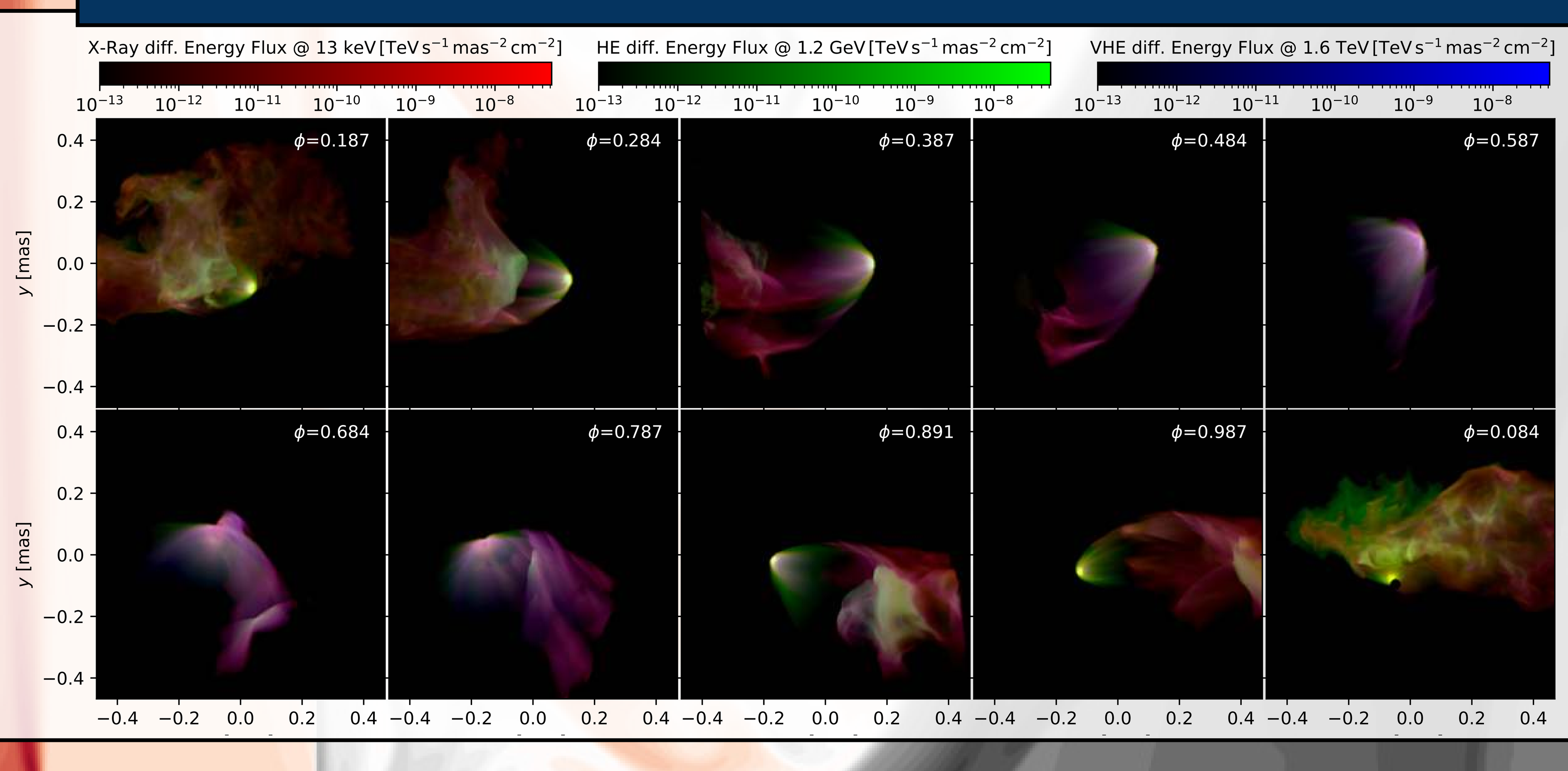

Fig 10: Projection of the predicted emission from LS 5039 for an observer at Earth for different orbital phases and inclination $i = 60°$. [2]